Materials Physics and Mechanics 38 (2018) 1-10 Received: March 16, 2018

DESIGN AND MANUFACTURING OF TAILORED MICROSTRUCTURE WITH SELECTIVE LASER MELTING

A.A. Popovich, V.Sh. Sufiiarov*, E.V. Borisov, I.A. Polozov, D.V. Masaylo

National Technology Initiative Center of Excellence in Advanced Manufacturing Technologies at Peter the Great St. Petersburg Polytechnic University, Russia, 195251, St.Petersburg, Polytechnicheskaya, 29

*e-mail: vadim.spbstu@yandex.ru

Abstract. The current paper presents the results of a complex investigation of effect of Selective Laser Melting process parameters on microstructure and properties of Inconel 718 bulk specimens. The possibility of obtaining bulk specimens with tailored microstructure was studied. The specimens with tailored microstructure were obtained and studied. It was shown that after heat treatment and hot isostatic pressing the differences in microstructure and mechanical properties of fine-grained and coarse-grained areas still remain in place. Finally, the feasibility of applying the developed approach was shown by manufacturing a gas-turbine engine blade with tailored microstructure in specific areas.

Keywords: additive manufacturing; selective laser melting; Inconel 718; EBSD; turbine blade, tailored microstructure.

1. Introduction

Selective Laser Melting (SLM) process is nowadays considered to be as one of the most advanced technologies among metal additive manufacturing processes [1-3]. SLM is already used for manufacturing metal parts, which is due to possibility of producing parts with a shape as close as possible to the final product. The latter is especially important in such areas as aviation and medicine [4-7]. The aviation, where titanium and nickel-based alloys are widely used, imposes specific requirements for the parts. Applying additive manufacturing allows creating parts with a geometry that simultaneously provides light-weight and high mechanical properties [4].

Inconel 718 nickel-based alloy attracts high attention among researchers due to its wide use in gas turbines, aerospace parts, petrochemical and nuclear industries, which resulted from its thermal stability and high-temperature properties [8]. Conventionally Inconel 718 parts are produced by forging, rolling and casting. However, in order to advance the modern manufacturing industry, it is necessary to create a manufacturing of complex metal parts with high precision and mechanical properties, which are sometimes not possible to achieve by conventional methods.

There are some studies in the literature that investigate the SLM process of Inconel 718 alloy, where the effect of process parameters on material's relative density has been studied. However, usually they put a focus on only laser power and scanning speed, while other parameters are kept fixed [9-13]. In order to control the SLM process, it is necessary to understand an influence pattern of a particular parameter on the final results. Nevertheless, not enough information has been published on a possibility of using SLM particularities as a means to create a specific crystallographic structure and grain size. Also, few information can be found about the relation of anisotropy, microstructure and mechanical properties of the

http://dx.doi.org/10.18720/MPM.3812018_1

alloy [14-18]. Therefore, the aim of this work is to determine the relation between obtained microstructure from the initial process parameters and to develop a method for production of bulk parts with tailored microstructure and study their properties, as well.

2. Materials and Methods

The bulk specimens were manufactured using a SLM 280HL machine (SLM Solutions GmbH, Germany). Gas atomized Inconel 718 heat-resistant alloy powder was used as the raw material. The measured chemical composition of the Inconel 718 powder is presented in Table 1.

Table 1. The chemical composition of Inconel 718 powder particles measured by energy dispersive X-ray spectroscopy.

Element	Ni	Cr	Fe	Nb	Mo	Ti	Al	Co	Mn
Content, wt%	51.4	19.4	18.5	5.3	3.4	1.0	0.7	0.1	0.1

The particle size distribution was measured using laser diffraction method with Analysette 22 NanoTecPlus device with a full-scale range of 0.01–2000 μm. The flowability of the powder was measured with a calibrated funnel (Hall Flowmeter). The surface morphology, microstructure of powder particles, as well as microstructure of the bulk specimens, texture characterization (EBSD) were investigated using scanning electron microscope (SEM) TESCAN Mira 3 LMU. EBSD analyses was carried out with the accelerating voltage of 20 kV and 5 μm step. The X-ray diffraction analysis was carried out using Bruker D8 Advance diffractometer. The mechanical properties were analyzed in accordance with ISO 6892-1 using Zwick/Roell Z100 testing machine. The relative density of bulk samples was measured by metallographical method and the Archimedes principle. Hot isostatic pressing (HIP) was carried out in an Avure Quintus at temperature of 1180ºC and pressure of 150 MPa during 3 hours. Heat treatment was carried out in two steps: 1) solution annealing at 1065ºC for 1 hour with air cooling; 2) two step aging: holding at 760ºC for 10 hours, then cooling to 650ºC for 2 hours and holding at 650ºC for 8 hours following air cooling.

3. Results and Discussion

SEM investigation of Inconel 718 powder (Fig. 1) showed that the powder particles have shape close to spherical. Some particles have satellites attached to them (Fig. 1, b). The presence of such particles is typical for gas atomized powder. The surface morphology of the particles features some roughness, which represents the casted microstructure and belongs to cellular-dendritic type of crystallization [19].

a) b)

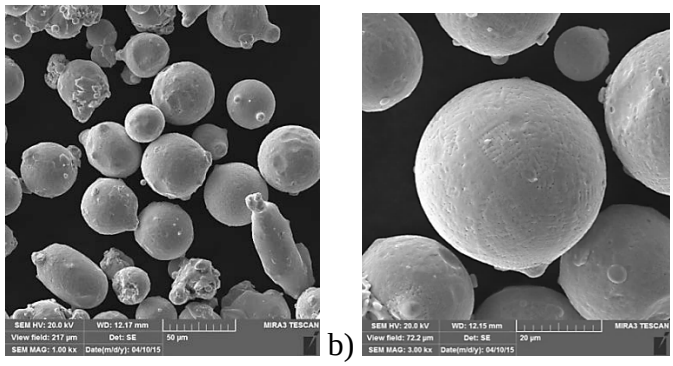

Fig. 1. SEM-images of Inconel 718 alloy powder particles produce by gas atomization: a) general view; b) particle's surface morphology.

In order to determine the correlation between SLM process parameters and bulk samples relative density, some researcher use such characteristic as energy density, but different equations are used. Some use linear energy density [7], others – volume energy density [8]. The authors of this work consider volume energy density to be a value that is more appropriate to estimate specific heat input. The main process parameters responsible for parts density can be grouped in a volume energy density E (J/mm^3) equation:

$$E=P/Vht, \quad (1)$$

where P – laser power (Wt), V – scanning speed (mm/s), h – hatch distance (mm), t – layer thickness (mm).

The summarized results of bulk samples relative density measurements, obtained with a fixed layer thickness of 30 μm at different volume energy density, are shown in Fig. 2.

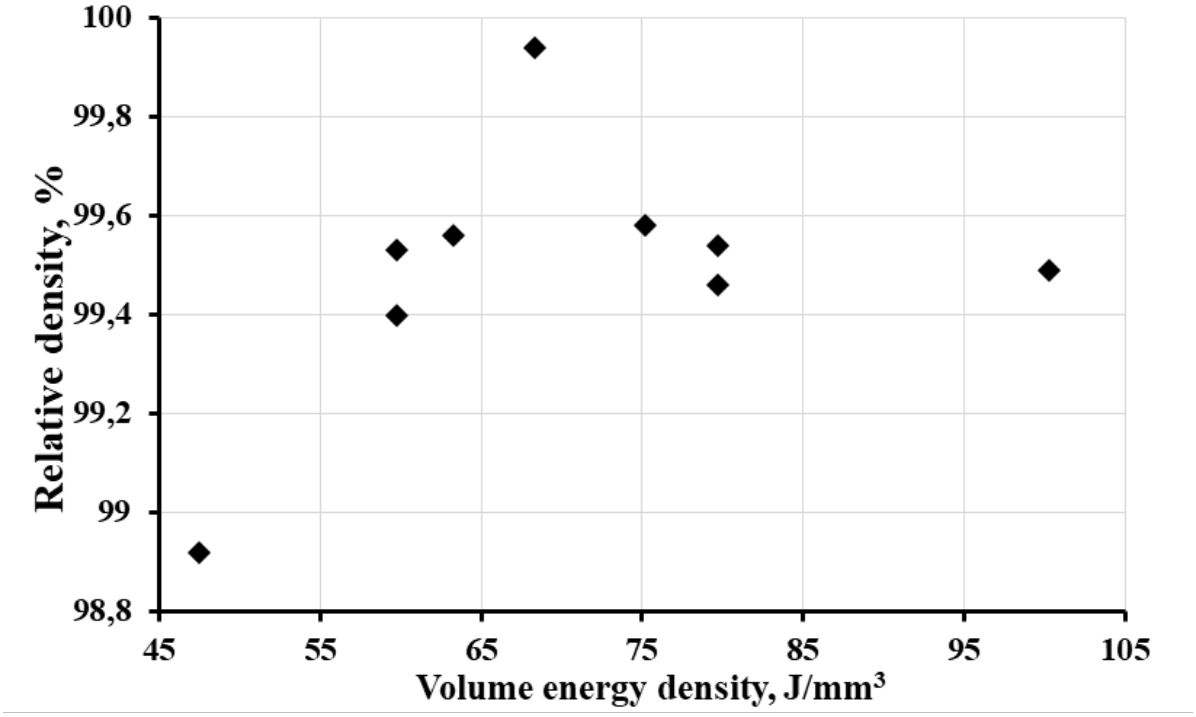

Fig. 2. Bulk samples relative density dependence on volume energy density.

The highest density, measured by the Archimedes principle, was determined for the sample obtained at 63.3 J/mm^3 energy density. The sample with the lowest density was produced at low energy density (47.5 J/mm^3), which resulted in insufficient melting of particles and joining the current layer with the previous one.

The process parameters, which resulted in the highest density of the samples at 30 μm layer thickness, and process parameters with identical energy density and layer thickness 50 μm and 100 μm were used to obtain samples for studying microstructure, phase composition and mechanical properties.

Due to fast cooling rates during SLM process (10^4–10^6 K/s), the as-SLM microstructure features fine cellular dendrites. The crystallization rate and, consequently, the cells size depend on layer thickness used during the SLM process (Fig. 3).

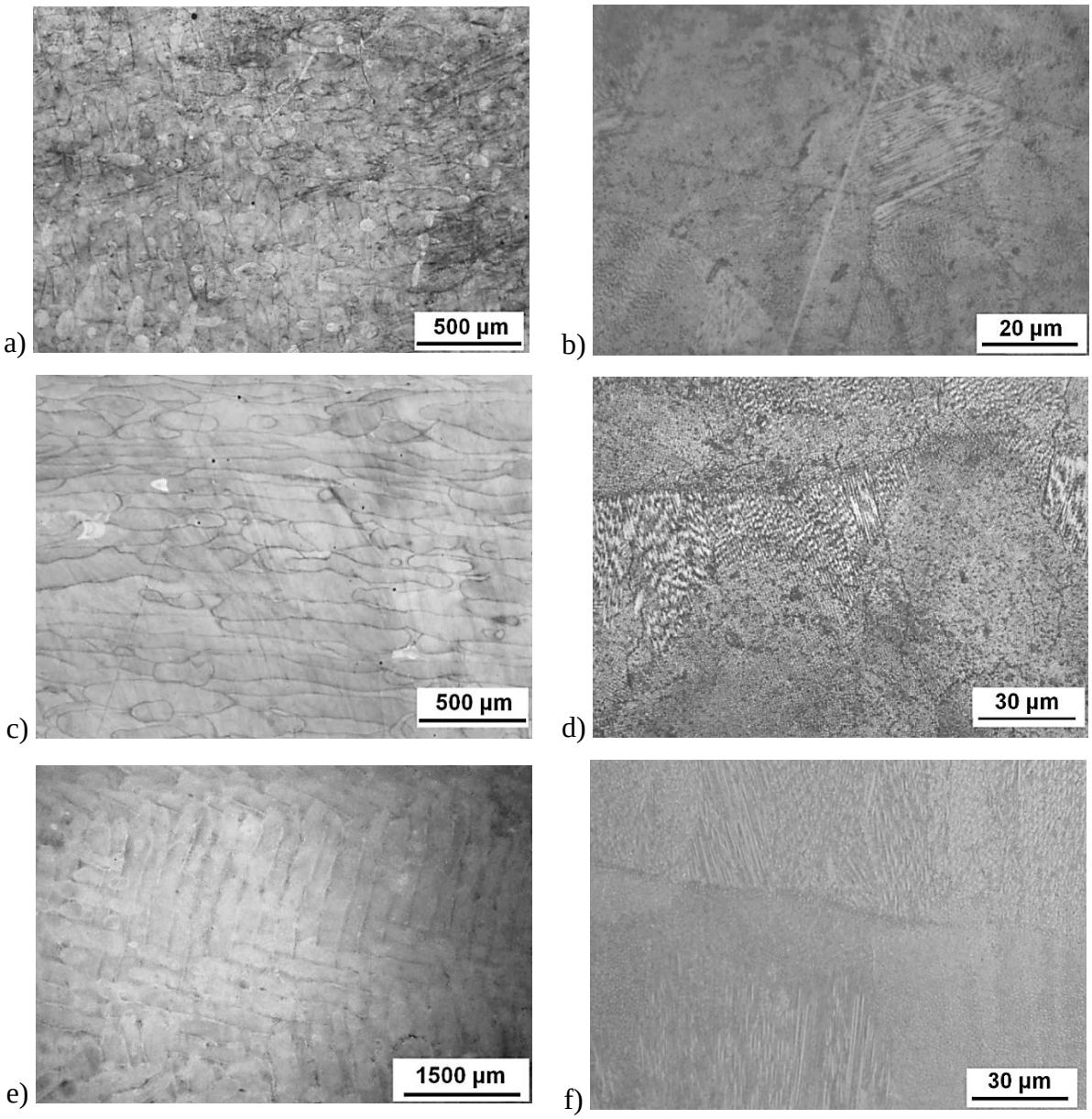

Fig. 3. Microstructures of the samples obtained by SLM at different layer thickness: (a, b) 30 μm, (c, d) 50 μm, and (e, f) 100 μm.

The average cell size at 30 μm layer thickness is 0.7–0.9 μm, at 50 μm layer thickness it is 0.9–1.1 μm, and at 100 μm layer thickness – 1.3–2.0 μm. The other differences at microstructure formation at different layer thicknesses are shown in Fig. 4, where the materials' crystallographic textures, studied with EBSD analysis, are shown.

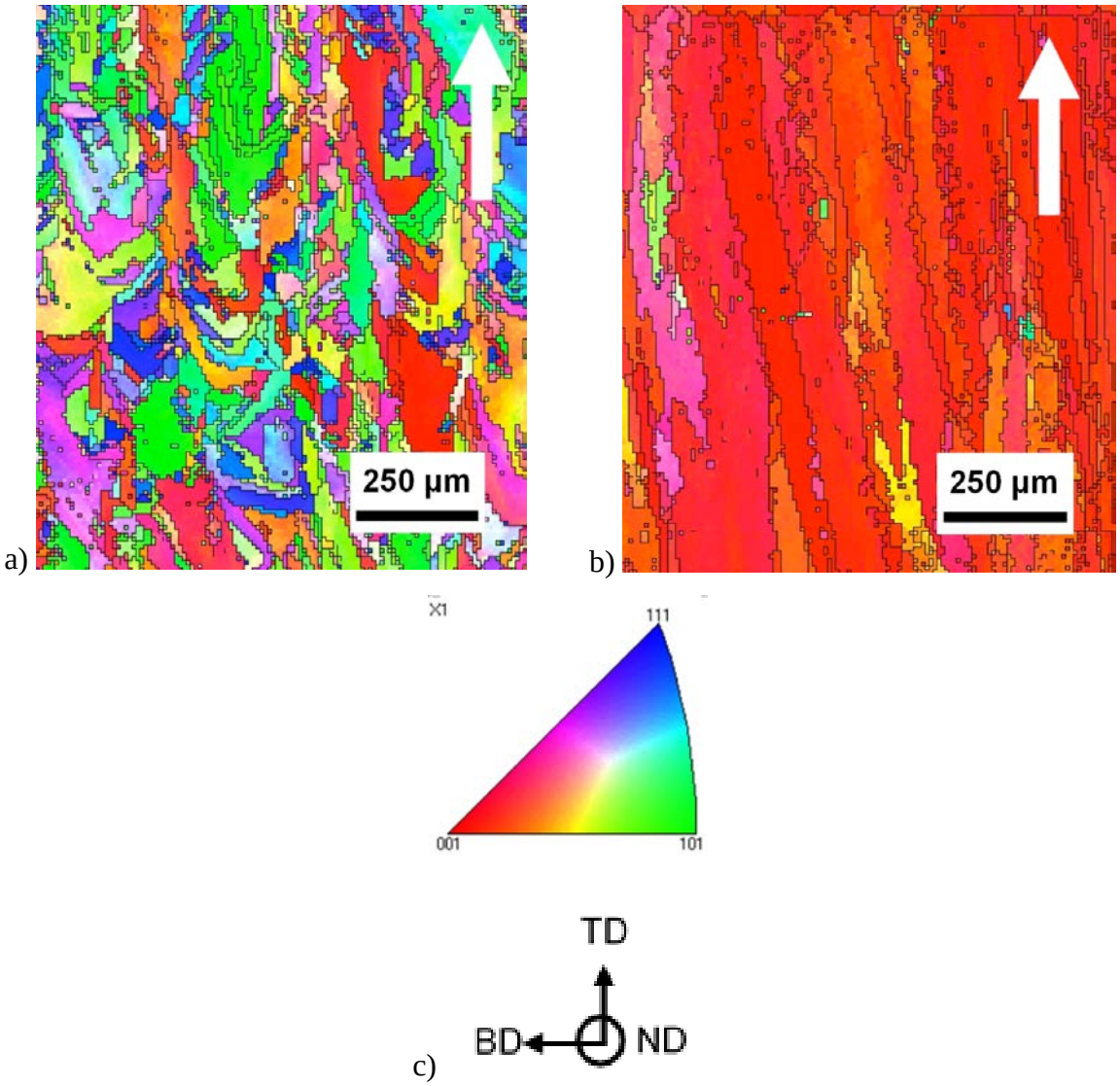

Fig. 4. EBSD analysis of the samples obtained by SLM:
a) inverse pole figure (IPF) for the samples produced at 50 µm layer thickness; b) IPF for the samples produced at 100 µm layer thickness; c) The index of IPF and the reference coordinate;
white arrows at figures a) and b) show building direction during SLM process.

The microstructure of the sample produced at 50 µm layer thickness features equiaxed grains with no predominant orientation, while the microstructure of sample obtained at 100 µm layer thickness has columnar grains with <001> predominant orientation.

The differences in microstructures should have an impact on mechanical characteristics of the material. In order to evaluate the tensile properties of the material, cylindrical specimens were produced to test the properties in accordance with ISO 6892-1. The information about yield strength, tensile strength and elongation at break for the produced specimens are shown in Table 2.

After solution annealing and aging the mechanical properties are much higher than in the non-heat-treated state (see Table 2). This was caused by phase composition change, specifically precipitation of γ''-Ni_3Nb strengthening phase. After HIP the strength properties decreased due to coarsening of the grains at elevated temperatures, however HIP treatment resulted in higher elongation of the material.

Table 2. The results of tensile tests at room temperature for Inconel 718 specimens obtained by SLM.

Layer thickness, μm	Yield strength, MPa	Tensile strength, MPa	Elongation at break, %
SLM			
50	650 ± 11	845 ± 9	28 ± 4
100	543 ± 2	782 ± 6	31 ± 6
SLM + HIP			
50	645 ± 6	1025 ± 14	38 ± 1
100	481 ± 11	788 ± 12	34 ± 3
SLM + HIP + Solution annealing + Aging			
30	1157 ± 13	1363 ± 12	21 ± 1
50	1145 ± 16	1376 ± 14	19 ± 1
100	1065 ± 20	1272 ± 12	15 ± 4
Casted [20]	488	786	11
Hot rolled, grain size ~40 μm [15]	1245	1415	24
Hot rolled, grain size ~100 μm [15]	1145	1290	24

High-temperature properties are important characteristics for superalloys. Inconel 718 parts are usually not utilized for long times at temperatures higher than 650ºC. Table 3 presents the results of tensile tests at 650ºC, carried out in accordance with ISO 6892-2, for the specimens with and without heat treatment and HIP.

Table 3. The results of tensile tests at 650ºC for Inconel 718 SLM specimens after HIP and heat treatment.

Layer thickness, μm	Yield strength, MPa	Tensile strength, MPa	Elongation at break, %
SLM			
30	716 ± 11	828 ± 9	27 ± 4
50	650 ± 11	845 ± 9	28 ± 4
100	543 ± 2	782 ± 6	31 ± 6
SLM + HIP			
50	626 ± 8	857 ± 14	29 ± 1
100	479 ± 5	665 ± 7	28 ± 2
SLM + HIP + Solution annealing + Aging			
50	942 ± 11	1078 ± 8	20 ± 2
100	872 ± 13	1005 ± 12	17 ± 4

The results of mechanical tests at elevated temperature showed stable results with the elongation at break about 30% for SLM and SLM + HIP specimens. The specimens after HIP and subsequent solution annealing and aging have lower elongation at break compared to other specimens.

Comparing the results of mechanical tests at room and elevated temperatures for the specimens obtained at different layer thicknesses and with different post-treatment, it can be concluded that the lower layer thickness leads to higher strength.

Designing and manufacturing of samples with tailored microstructure. The next step was to develop an approach to manufacture specimens with tailored microstructure in specific areas. In order to produce different areas of the specimens, 50 μm and 100 μm layer thicknesses were used in those areas. Different combinations of these areas in the bulk specimens were used in order to determine a possibility of their spatial variation in the final part. The produced samples are shown in Fig. 5.

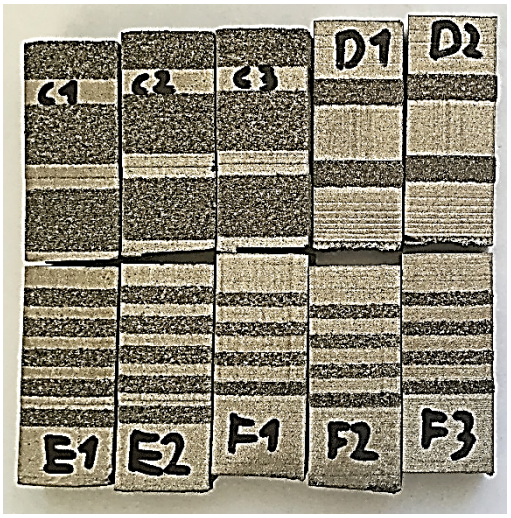

Fig. 5. The specimens with tailored microstructure areas. The dark areas correspond to 100 μm layer thickness, the light areas correspond to 50 μm layer thickness.

EBSD-analysis of the specimens (Fig. 6) shows that on the boundary of different areas a mutual penetration of fine-grained and coarse-grained areas can be seen there, thus a transition area is present in the specimen. Its size is about 500 μm depending on mutual arrangement of fine-grained and coarse-grained areas.

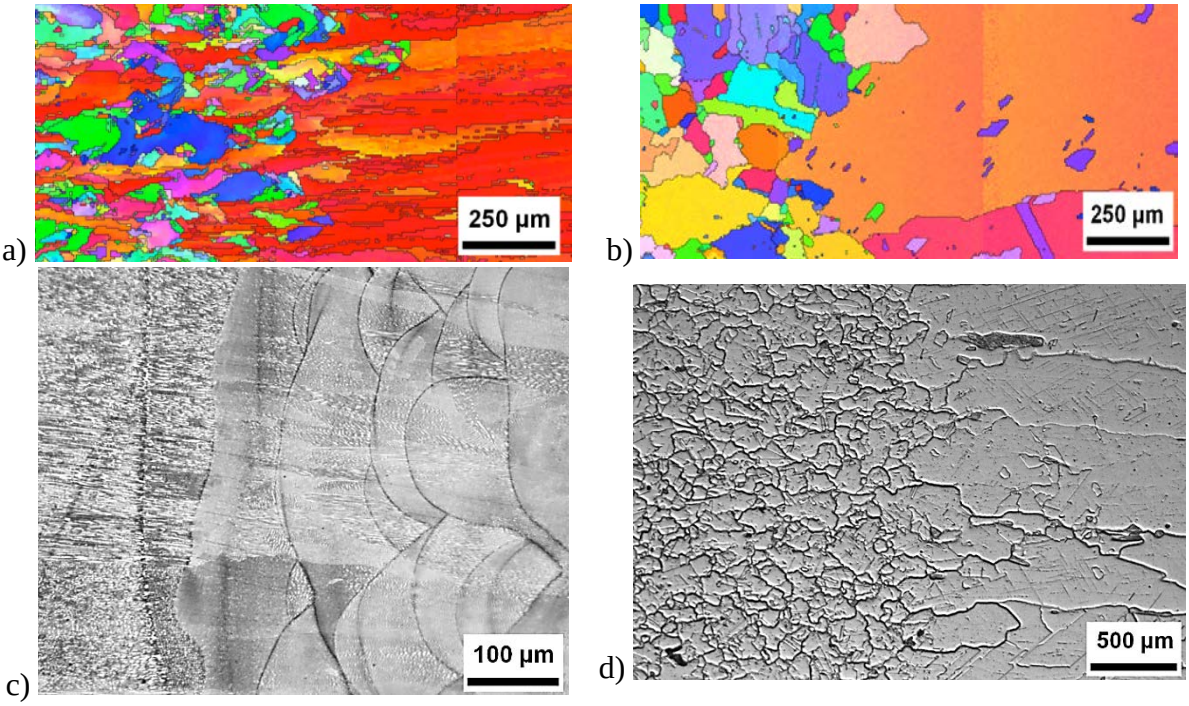

Fig. 6. Microstructure of the transition region between areas produced at 50 μm (left) and 100 μm (right) layer thicknesses after SLM (a, c) and SLM+HIP (b, d).

The effect of HIP on the microstructure can be seen in Fig. 6. Heating above recrystallization temperature point resulted in coarsening of the grains and formation of equiaxed grains in the 50 μm layer thickness area. Thus, formation of two regions occurs after heat treatment – a region of directional columnar grains and a region of fine equiaxed grains. There is NbC carbide network around those grains (Fig. 7).

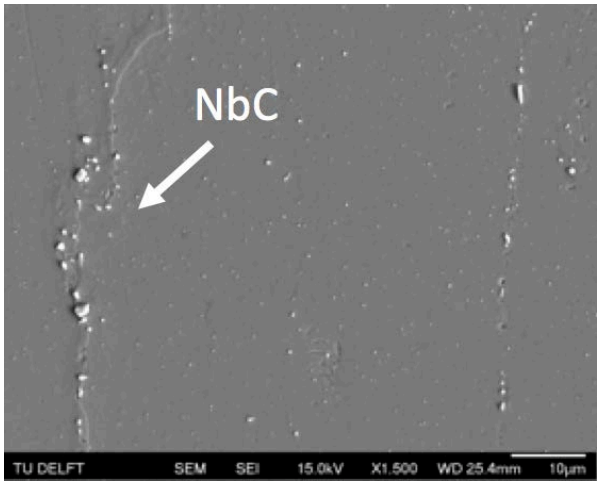

Fig. 7. SEM-image showing the presence of carbides in the bulk material.

The presence of carbides inhibits grain growth during the HIP and heat treatment, and also contributes to strengthening of the material [20].

Figure 8 shows the results of hardness measurements for specimens with tailored microstructure after SLM.

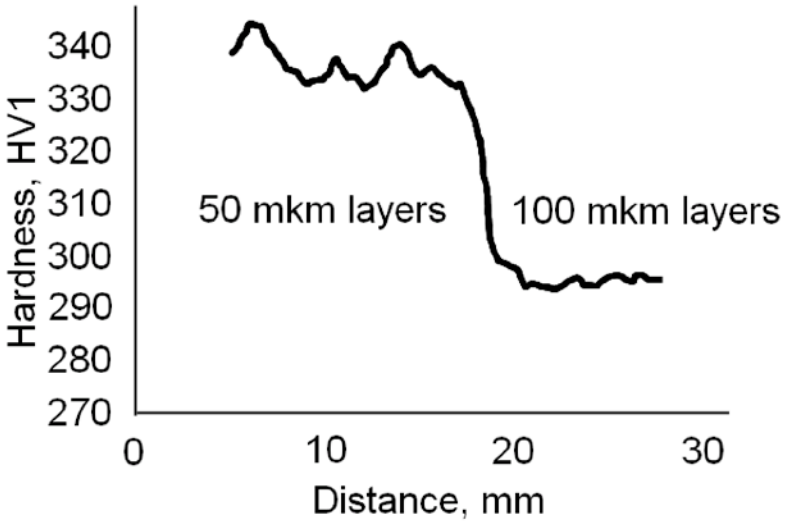

Fig. 8. Hardness of the specimens with tailored microstructure.

It can be seen that there is about 20% difference in hardness values between areas produced at different layer thicknesses. Equiaxed grain region has higher hardness than columnar grain region.

It is known that in order to improve the performance of turbine blades and vanes, dedicated methods of directional solidification can be applied to form a columnar or a monocrystalline structure. According to literature data, this kind of structure improves creep resistance of the materials, but at the same time has lower fatigue strength compared to a finely dispersed equiaxed microstructure.

There are two major elements in a turbine blade: a blade airfoil and a blade root. A blade airfoil works for a long time at high temperature and is under significant stress due to the effect of centrifugal forces. Thus, creep resistance is the most critical property for this part of the blade. At the same time, the blade root works at lower temperatures and is under multidirectional load. For this reason, fatigue resistance is the most critical for the blade root.

From the above reasoning, an approach for producing a prototype of a turbine blade with controlled microstructural areas by selective laser melting has been developed. For manufacturing of the blade root section, we used SLM process parameters that allow to obtain equiaxed fine-grained microstructure (50 μm layer thickness). The blade airfoil portion was produced at 100 μm layer thickness in order to obtain directed columnar grains with <001> orientation. Fig. 9 shows the photograph of the produced blade and its microstructure along the blade's section.

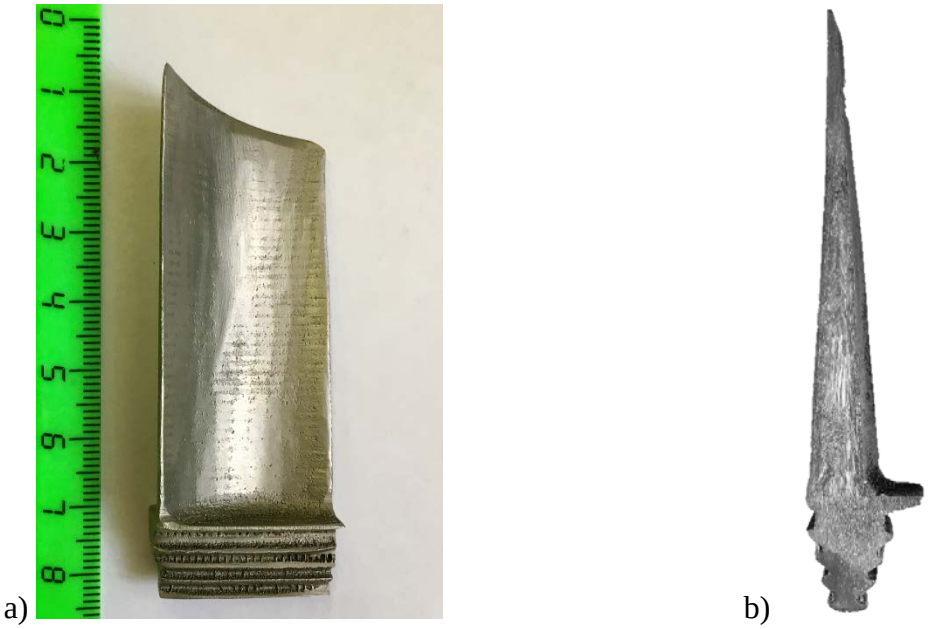

a) b)

Fig. 9. The photograph of the produced blade (a) and its microstructure (b).

Thus, it is possible to control the formation of microstructure at specific regions of the part in order to provide the required properties depending on the load conditions.

4. Conclusions

The results of complex investigation of selective laser melting process of Inconel 718 powder is presented in the paper. The effect of process parameters on the relative density of bulk samples was shown. It was shown that higher layer thickness leads to bigger cells size in the microstructure of the bulk Inconel 718 alloy samles. EBSD analysis showed that varying layer thickness leads to changing the grains' morphology. Using higher layer thickness, it is possible to implement a solidification of direct columnar grains during selective laser melting process. The mechanical properties of the specimens depend on the layer thickness: lower layer thickness leads to higher strength. The results of microstructure studies of the samples with alternate areas of fine and coarse grains were presented. Hardness measurements showed the local changes in mechanical properties. Based on the carried out investigation, an approach for manufacturing parts with controlled microstructural areas was proposed. Using a turbine blade as an example, the possibility of manufacturing complex-shaped parts with tailored microstructure and properties by selective laser melting was shown.

Acknowledgments. *The work was carried out with the funding from the Federal Target Program «Research and Development in Priority Areas for the Development of the Russian Science and Technology Complex for 2014-2020». The unique identifier of the project RFMEFI57817X0245.*

References

[1] T. Wohlers, *Wohlers Report 2017: Additive Manufacturing and 3D Printing State of the Industry - Annual Worldwide Progress Report* (Wohlers Associates, Inc., Colorado, 2017).
[2] M.J. Holzweissig, A. Taube, F. Brenne, M. Schaper, T. Niendorf // *Metallurgical and Materials Transactions B* **545** (2015) 46.
[3] A. Popovich, V. Sufiiarov, In: *Metal Powder Additive Manufacturing*, ed. by I. Shishkovsky (InTech, 2016), Vol. 10, p.215.
[4] A. Popovich, V. Sufiiarov, I. Polozov, E. Borisov, D. Masaylo // *METAL 2016 - 25th Anniversary International Conference on Metallurgy and Materials Conference Proceedings* (2016) 1504.
[5] D.F. Paulonis, J.J. Schirra // *Superalloys* **718** (2001) 13.
[6] A.K. Abraham, V.G. Sridhar // *Trends in Biomaterials & Artificial Organs* **29(3)** (2015) 258.
[7] W.E. Frazier // *Journal of Materials Engineering and Performance* **23** (2014) 1917.
[8] V.Sh. Sufiiarov, A.A. Popovich, E.V. Borisov, I.A. Polozov // *Tsvetnye Metally* **1** (2017) 77.
[9] K.N. Amato, S.M. Gaytan, L.E. Murr, E. Martinez, P.W. Shindo, J. Hernandez, S. Collins, F. Medina // *Acta Materialia* **60** (2012) 2229.
[10] Q. Jia, D. Gu // *Journal of Alloys and Compounds* **585** (2014) 713.
[11] R. Wauthle, B. Vrancken, B. Beynaerts, K. Jorissen, J. Schrooten, J.P. Kruth, J. Van Humbeeck // *Additive Manufacturing* **5** (2015) 77.
[12] V.G. Smelov, A.V. Sotov, A.V. Agapovichev // *Chernye Metally* **9** (2016) 61.
[13] J. Strößner, M. Terock, U. Glatzel // *Advanced Engineering Materials* **17** (2015) 1099.
[14] H. Meier, C. Haberland // *Materialwissenschaft und Werkstofftechnik* **39** (2008) 665.
[15] J.P. Pedron, A. Pineau // *Materials science and engineering* **56** (1982) 143.
[16] S. Bai, L. Yang, J. Liu // *Applied Physics A* **122** (2016) 1.
[17] T. Niendorf, F. Brenne, M. Schaper, W. Reimche // *Rapid Prototyping Journal* **22** (2016) 630.
[18] A.V. Agapovichev, V.V. Kokareva, V.G. Smelov, A.V. Sotov // *IOP Conference Series: Materials Science and Engineering* **156** (2016) 012031.
[19] V.M. Golod, V.Sh. Sufiiarov // *IOP Conference Series: Materials Science and Engineering* **192** (2017) 012009.
[20] B. Baufeld // *Journal of materials engineering and performance* **21** (2012) 1416.